Pharmacokinetics and pharmacodynamics of remimazolam (CNS7056) after continuous infusion in healthy male volunteers: Part II. Pharmacodynamics of EEG effects

Supplemental Digital Content

S1: Recording and processing of the multichannel EEG data

The raw EEG signal was recorded with a 6-channel neurophysiologic system (Natus-Nicolet V32 with Software Neuroworks 8.4.0, Natus Europe, Planegg, Germany). Before placement of the EEG electrodes at C3, C4, F3, F4, O1, O2, Cz (reference), and Fp1 (ground) according to the international 10/20 system, the skin was prepared with abrasive gel (Everi, GVB-geliMED, Bad Segeberg, Germany) to keep impedances below 10 kΩ. Reusable Cup Electrodes (GVB-geliMED, Bad Segeberg, Germany) in silver chloride (AgCl) with silicone cable (250 cm length) were placed at the mentioned position via an EEG Cap (MultiCap Base, GVB-geliMED, Bad Segeberg, Germany) of appropriate size. A conductive gel (Neurgel, GVB-geliMED, Bad Segeberg, Germany) was injected through the cup electrodes. The analog EEG signal was digitized at a rate of 500 Hz with a gain of 0.1525902 µV/unit by the Natus Software and stored as EDF files on hard disk for further processing.

Using the open source software package "edfReader" for R (Version 1.1.2, 2017) , the digitized EEG signals were extracted from the EDF files and stored as a binary file (2 byte signed integer per voltage value) for each channel. The raw EEG signal of each EEG channel was first low-pass filtered via a finite impulse response at 47 Hz (preserves phase information needed for bispectral analysis), down sampled to 125 Hz, and subsequently high-pass filtered with a finite impulse response filter at 0.5 Hz (Matlab Signal Processing Toolbox, Release 7.1, Math-Works Inc., Natick, MA).

The preprocessed EEG signal was first segmented into epochs of 8.192 s (1024 data points) length (Matlab R2015b, Math-Works Inc., Natick, MA). These EEG signal epochs were first evaluated for signal quality (automatic neural networks based artifact recognition) and

stationarity (i.e., whether the statistical properties of the EEG signal epoch are time invariant using a non-parametric 'run'-test) after removal of DC offset.

The power spectrum estimates between 0.5 Hz and 5 Hz (delta), 5 Hz and 8 Hz (theta), 8 Hz 13Hz (alpha), 13Hz 26 Hz (beta), and 26 Hz 47 Hz (gamma) frequency bands (frequency range from > lower threshold to ≤ higher threshold) were computed from artifact free stationary EEG epochs using the squared absolute Fourier transform coefficients scaled by the length of the epoch. The Fourier coefficients for the corresponding frequency band of the time series were obtained with the Matlab command fft.m (Matlab Signal Processing Toolbox, Release 7.1, Math-Works Inc., Natick, MA).

Spectrograms were computed from unprocessed EEG epochs between 0.5 Hz and 40 Hz with a multitaper estimate of the power spectrum implemented in the Matlab command pmtm.m (Matlab Signal Processing Toolbox, Release 7.1, Math-Works Inc., Natick, MA) with the time-bandwidth product of 4 and a Fast Fourier Transform of the EEG epoch of 1024 samples. The number of tapers used to form the power spectrum density estimate was equal to two times the time-bandwidth product minus one, and the length of the estimated power spectrum was half of the EEG epoch length plus one.

From each EEG epoch, 38 univariate EEG variables were calculated as follows:

- From the distribution voltage values: the mean, standard deviation, skewness, kurtosis; electroencephalographic suppression ratio; the symbolic entropy[1], and the approximate entropy.[2]
- From the spectral power between 0.5 and 47 Hz: the 25th, 50th, 75th, 90th, and 95th quantiles; the spectral entropy[3]; the average absolute power and the absolute and relative power in the frequency range 0.5-2 Hz, 2-4 Hz, 4-8 Hz, 8-13 Hz, 13-20 Hz, 20-26 Hz, 26-32 Hz, and 32-47 Hz, (frequency range from > x to ≤y); the log ratio of power in frequency range 32-47 Hz to power in frequency range 0.5-2 Hz, 2-4 Hz, 4-8

Hz and 8-13 Hz, respectively; the log ratio of power in frequency range 30-47 Hz to power in frequency range 11-20 Hz (beta ratio).[4]

- From the bispectral plane of power between 0.5 and 47 Hz: the sum of bispectrum magnitude values and the sum of normalized bispectrum (bicoherence) magnitude values; the log ratio of the sum of bispectrum magnitude values in the frequency range 0.5-47 Hz to the sum of bispectrum magnitude values in the frequency range 40-47 Hz (SyncFastSlow measure).[5]

The time series of each EEG variable from each EEG channel was further processed for artifact rejection and smoothing. Each EEG variable value calculated from an EEG epoch lacking stationarity (i.e., alpha<0.05 probability of signal stationarity) and having a signal artifact content higher than 0.3 (0=no artifact, 1=artifact) was discarded from further analysis. The missing values of the time series of each EEG variable were replaced by linear interpolation. Afterwards, the time series of each EEG variable were smoothed by Tukey's Running Median Smoother.

1. Schurmann T, Grassberger P: Entropy estimation of symbol sequences. Chaos 1996; 6: 414-427

2. Bruhn J, Ropcke H, Hoeft A: Approximate entropy as an electroencephalographic measure of anesthetic drug effect during desflurane anesthesia. Anesthesiology 2000; 92: 715-26

3. Rezek IA, Roberts SJ: Stochastic complexity measures for physiological signal analysis. IEEE Trans Biomed Eng 1998; 45: 1186-91

4. Rampil IJ: A primer for EEG signal processing in anesthesia. Anesthesiology 1998; 89: 980-1002

5. Sigl JC, Chamoun NG: An introduction to bispectral analysis for the electroencephalogram. J Clin Monit 1994; 10: 392-404

S2: Selection of EEG parameters for pharmacodynamic modeling

In order to identify suitable EEG variables for the assessment of remimazolam-induced sedation, the derived EEG variables were further analyzed with respect to signal-to-noise ratio and prediction probability for MOAA/S scores.

For calculation of the signal-to-noise ratio, the time series of estimated and original EEG variables from EEG epochs during a time interval of 5 min before first MOAA/S score and 5 min after last MOAA/S score were selected for further analysis. The estimation technique included rejection of variable values calculated from nonstationary or artifact contaminated EEG epochs, linear interpolation of rejected values, and smoothing with the Tukey's Running Median Smoother. The smoothing procedure starts with a running median of 4 data samples, then 2, then 5, then 3 followed by a running weighted average, the weights being 0.25, 0.5, and 0.25. Signal-to-noise ratio was computed as the ratio between the variance of the estimated and the variance of residuals. Residuals were computed as the difference between estimated and measured (unprocessed) variable values. The population average signal-to-noise ratio values are presented in table S2T1.

For calculation of the prediction probability, pairs of estimated EEG variable values and MOAA/S scores were generated for each EEG variable from each channel in each volunteer. These pairs were composed of one MOAA/S score and one corresponding value of the smoothed EEG variable selected from the time interval of 35 s before the MOAA/S score observation to the time point of MOAA/S score observation. Subsequently, the relationship between the time course of the EEG variable and the time course of the MOAA/S scores was visually evaluated as concordant or discordant. A concordant relationship was present if EEG variable values and MOAA/S scores were rank ordered in the same direction, and a discordant relationship was present if they were rank ordered in opposite direction. The prediction probability of the EEG variable for the MOAA/S scores was calculated as:

$$P_k = \frac{P_c + \frac{1}{2} P_{tx}}{P_c + P_d + P_{tx}}$$

where P_c and P_d are the probabilities for a concordant and discordant relationship, respectively. The probability that the EEG variable does not change although underlying changes in MOAA/S scores is given by P_{tx}. The P_k value ranges from 0 to 1, whereas 0 indicates a perfect discordant and 1 a perfect concordant relationship. P_k equals 0.5 when the probability of discordance or concordance is not better than random guess. In order to compare the P_k values of all EEG variables independent of their type of relationship to the MOAA/S scores, the P_k of the EEG variable was calculated as 1-P_k in case of a discordant relationship. For each volunteer, the P_k values were calculated from all timely associated value pairs of EEG measure and MOAA/S score, independent of their time of occurrence. The population mean P_k values are presented in table T1.

Table S2T1: Population signal-to-noise ratios and prediction probabilities of 38 EEG variables. SNR: signal-to-noise ratio, P_k: prediction probability

		C3		C4		F3		F4		O1		O2	
Variable	Specification	SNR	P_k	SNR	P_k	SNR	P_k	SNR	P_k	SNR	P_k	SNR	P_k
mean_amp	mean absolute amplitude	0.43	0.8	0.65	0.81	0.87	0.82	0.97	0.82	0.32	0.72	0.01	0.78
avPower	average absolute power	0.1	0.79	0.14	0.8	0.24	0.82	0.27	0.82	0.05	0.71	0.07	0.78
stddev	standard deviation of voltage distribution	0.35	0.79	0.5	0.8	0.73	0.82	0.8	0.82	0.3	0.71	0.2	0.77
skew	skewness of voltage histogram	0.11	0.57	0.12	0.56	0.27	0.37	0.24	0.39	0.19	0.6	0.07	0.65
kurt	kurtosis of voltage histogram	0.07	0.72	0.06	0.7	0.11	0.69	0.09	0.67	0.08	0.69	0.79	0.64
q25	25th quantile of power distribution	0.8	0.71	0.72	0.72	0.28	0.68	0.32	0.68	0.83	0.72	1.61	0.67
q50	50th quantile of power distribution	1.97	0.69	2.1	0.7	1.51	0.66	1.61	0.67	1.79	0.69	1.17	0.65
q75	75th quantile of power distribution	1.16	0.71	1.07	0.7	1.13	0.68	1.18	0.69	1.31	0.67	0.71	0.64
q90	90th quantile of power distribution	1.19	0.73	1.08	0.73	1.35	0.75	1.19	0.75	1.13	0.71	1.24	0.66
q95	95th quantile of power distribution	1.82	0.74	1.74	0.75	2.22	0.77	1.86	0.77	2.08	0.73	0	0.69
abs05-2	power 0.5-2 Hz	0.09	0.77	0.1	0.77	0.13	0.76	0.14	0.77	0.04	0.7	0.02	0.76
abs2-5	power 2-5 Hz	0.06	0.76	0.18	0.78	0.22	0.75	0.26	0.78	0.12	0.72	0.11	0.75
abs5-8	power 5-8 Hz	0.18	0.63	0.24	0.66	0.49	0.7	0.54	0.74	0.19	0.56	0.52	0.6
abs8-13	power 8-13 Hz	0.94	0.72	1.06	0.71	1.57	0.81	1.43	0.81	0.63	0.67	1.21	0.73
abs13-20	power 13-20 Hz	1.74	0.53	2.26	0.53	2.1	0.61	1.58	0.63	1.34	0.52	0.87	0.57

abs20-26	power 20-26 Hz	1.08	0.55	1.15	0.55	0.97	0.56	0.91	0.57	1.11	0.55	0.31	0.51
abs26-32	power 26-32 Hz	0.57	0.52	0.55	0.51	0.37	0.52	0.32	0.52	0.42	0.56	0.13	0.51
abs32-47	power 32-47 Hz	0.12	0.58	0.13	0.56	0.1	0.53	0.08	0.56	0.26	0.65	1	0.61
rel05-2	ratio power 0.5-2 Hz to power 0.5-47 Hz	1.41	0.7	1.42	0.7	1.08	0.63	1.16	0.64	1.1	0.69	0.48	0.66
rel2-5	ratio power 2-5 Hz to power 0.5-47 Hz	0.46	0.43	0.45	0.43	0.86	0.38	0.93	0.39	0.56	0.41	1.02	0.47
rel5-8	ratio power 5-8 Hz to power 0.5-47 Hz	1.05	0.29	0.94	0.28	0.95	0.34	0.88	0.35	1.16	0.26	1.2	0.29
rel8-13	ratio power 8-13 Hz to power 0.5-47 Hz	1.52	0.45	1.74	0.43	1.18	0.62	1.24	0.6	1.27	0.46	1.68	0.44
rel13-20	ratio power 13-20 Hz to power 0.5-47 Hz	2.59	0.36	2.5	0.35	2.32	0.39	2.51	0.38	1.83	0.39	1.54	0.37
rel20-26	ratio power 20-26 Hz to power 0.5-47 Hz	1.71	0.71	1.85	0.72	1.64	0.75	1.77	0.75	1.75	0.71	1.3	0.68
rel26-32	ratio power 26-32 Hz to power 0.5-47 Hz	1.17	0.75	1.13	0.74	1.27	0.77	1.14	0.78	1.59	0.74	1.12	0.69
rel32-47	ratio power 32-47 Hz to power 0.5-47 Hz	0.95	0.77	0.59	0.76	1.12	0.79	0.62	0.79	1.95	0.78	1.67	0.72
dbr	ratio power 32-47 Hz to power 0.5-2 Hz	1.8	0.75	1.96	0.75	2.06	0.75	2	0.76	2.41	0.76	1.52	0.72
tbr1	ratio power 32-47 Hz to power 2-5 Hz	1.26	0.74	1.23	0.75	1.34	0.74	1.25	0.75	1.97	0.76	1.11	0.73
tbr2	ratio power 32-47 Hz to power 5-8 Hz	1.21	0.69	1	0.67	1.6	0.72	1.57	0.72	1.86	0.67	2.1	0.62
abr	ratio power 32-47 Hz to power 8-13 Hz	2.12	0.75	1.98	0.73	3.48	0.8	3.26	0.79	3.68	0.76	1.25	0.71
symbentrop	symbolic entropy of voltage	1.87	0.79	2.11	0.8	2.4	0.83	3	0.82	1.45	0.74	0.8	0.78
specentrop	spectral entropy of power 0.5-47 Hz	1.17	0.72	1.22	0.73	1.02	0.71	1.22	0.72	1.04	0.72	1.01	0.67
ae1	approximate entropy	1.28	0.73	1.34	0.73	1.64	0.76	1.68	0.77	1.44	0.68	0.06	0.71
bic	sum of bicoherence magnitude over 0.5-47 Hz	0.01	0.49	0.03	0.51	0.02	0.52	0.01	0.49	0.02	0.57	2.78	0.54
bispec	sum of bispectrum magnitude over 0.5-47 Hz	0.1	0.75	0.16	0.78	0.27	0.79	0.25	0.81	0.06	0.72	0.22	0.77
beta_ratio	log ratio of power 30-47 Hz to power 11-20 Hz	2.7	0.7	2.51	0.71	4.29	0.79	4.04	0.8	4.21	0.79	1.71	0.74
bic_sfs	log ratio of sum of bicoherence 0.5-47 Hz to sum of bicoherence 40-47 Hz	0.11	0.55	0.1	0.55	0.11	0.51	0.09	0.49	0.24	0.47	0.01	0.49
bispec_sfs	log ratio of sum of bispectrum 0.5-47 Hz to sum of bispectrum 40-47 Hz	1.55	0.72	1.4	0.73	1.78	0.77	1.65	0.78	2.68	0.77	0.07	0.71

S3: Methods of pharmacokinetic/-dynamic (PKPD) modeling

PKPD modeling was performed in a sequential approach: pharmacokinetics were analyzed first, and the individual empirical Bayesian estimates of the pharmacokinetic parameters were used in the pharmacodynamic analysis to estimate the plasma and effect site concentration at the time points where the dependent pharmacodynamic value (selected EEG variable or Narcotrend index) was measured. The pharmacokinetic modeling of remimazolam is described in detail in the accompanying part I of this study.

For the pharmacodynamic modeling of selected EEG variable and Narcotrend index, sigmoid inhibitory models with effect site compartment were used. The basic model of this type had the form:

$$E = E_0 - E_{max} \frac{C_E^\gamma}{C_E^\gamma + EC_{50}^\gamma} \quad \text{or}$$

$$E = E_0 - (E_0 - E_{min}) \frac{C_E^\gamma}{C_E^\gamma + EC_{50}^\gamma}$$

where E is the value of the EEG variable for an effect site concentration C_E, E_0 is the baseline value of the EEG variable when no drug is present, E_{max} is the maximum inhibitory effect and E_{min} is the minimum value of the EEG variable. The effect site concentration C_E was calculated from the plasma concentration (C_P) of remimazolam by the differential equation

$$\frac{dC_E}{dt} = k_{e0} \cdot (C_P - C_E)$$

using the individual empirical Bayesian estimates of the best pharmacokinetic model for remimazolam to calculate C_P.

Interindividual variability of the model parameters was modeled by normal or log-normal distributions. Residual intraindividual variability was modeled using an additive error model.

Parameters were estimated using NONMEM (Version 7.4.1, ICON plc, Ireland) and the first-order conditional estimation method with interaction (FOCE-I) algorithm.

Model Development

Modeling was performed sequentially: The basic structural model was determined first, followed by covariate analysis. Selection of the best structural model was primarily based on the Bayes information criterion (BIC) defined as BIC=OFV+ln(Nobs)*Npar, where OFV is the NONMEM objective function value to be minimized, Nobs is the number of observations and Npar is the number of parameters to be estimated. The model with the lowest BIC was selected as best model.

After the structural model had been selected, the individual Bayesian estimates of the model parameters were used for the detection of covariate effects. The informativeness of the individual Bayesian estimates was assessed by the η-shrinkage of the model parameters, defined as 1 - SD(η_i)/ω, where η_i are the individual Bayesian estimates of interindividual variance and ω is the population model estimate of the corresponding standard deviation. For detection of covariate effects, the individual Bayesian estimates of the model parameters were plotted independently against age and weight. Linear regression analysis was used as a first test for covariate effects. Subsequently, selected covariates were incorporated into the basic structural model using linear relationships with centering on the median value of the covariate (COV) within the population:

$$\theta_i = \theta_{TV} + \theta_{COV} \cdot (COV - Median(COV))$$

where θ_{TV} is the typical value of the parameter in the population and θ_{COV} quantifies the covariate effect.

Covariate analysis was also primarily based on the BIC. A model with additional covariates was favored if the BIC was lower than for the model without covariates. The likelihood ratio

test (LRT) was also performed: the difference in the OFV was tested for significance by the chi-square test with the degree of freedom being equal to the difference in the number of model parameters. If the covariate model has one additional parameter more than the basic model, a decrease of OFV by more than 3.84 is significant with $p<0.05$. If a covariate model included additional parameters, it was also tested whether the 95% confidence interval of the additional parameters included the null hypothesis value. Covariates were included step-by-step starting from the basic structural model. Subsequently, backward deletion analysis was performed, testing each covariate effect for significance by fixing the corresponding parameter at θ_{COV}=0.

Model Evaluation and Validation

Diagnostic plots (measured values of an EEG variable vs. population predictions and vs. individual predictions, conditional weighted residuals vs. time and vs. population predictions) were used to assess goodness of fit. Additionally, we calculated for each measured value the prediction error (PE_{ij}) and the absolute prediction error (APE_{ij}):

$$PE_{ij} = E_{m,ij} - Ec_{p,ij}$$

$$APE_{ij} = |E_{m,ij} - Ec_{p,ij}|$$

where $E_{m,ij}$ is the jth measured value of the EEG variable of the i-th individual, and $E_{p,ij}$ is the corresponding predicted value. Prediction errors were calculated for individual and population predictions, and goodness of fit was assessed by the median values of PE_{ij} (MDPE) and APE_{ij} (MDAPE).

Models were further validated by visual predictive check with 1000 simulated datasets using the doses and sampling times of the original data set, and model parameters with distributions as determined in the final pharmacokinetic model.

Bootstrap analysis was performed to analyze the stability of the model and to obtain nonparametric confidence intervals of the final population model parameters. From the observed data, 1000 new data sets with the same number of individuals as the original data set were generated by resampling with replacement, and the final model was fitted to these new data sets.

The reliability of the parameter estimates was further assessed by log-likelihood profiling (LLP). For this purpose, the parameter to be assessed was fixed at particular values around its final population estimate, and the corresponding OFV values were plotted vs. the parameter values. This profile should have a clear minimum at the final estimate and its shape should not be too flat. As the change of the OFV follows approximately a chi-square distribution with one degree of freedom, nonparametric 95% and 99% confidence intervals of the parameter are defined by those areas of the likelihood profile where $\Delta OFV < 3.84$ and <6.63, respectively.

S4: Sample size estimation

Although this was an explanatory and not a confirmation study, we performed some sample size estimation with respect to pharmacodynamic modeling of the Narcotrend index, because of lack of data regarding EEG measures from spontaneous EEG. For pharmacodynamic modeling, sample size was estimated by simulation. For the pharmacodynamics of remimazolam with respect to the Narcotrend index, there were only few unpublished data available. Based on these data and using the infusion scheme of the present study, we simulated Narcotrend index data for populations of 10, 15 and 20 subjects, assuming a three-compartment model for pharmacokinetics and a sigmoid E_{max} model with effect site compartment for pharmacodynamics. Pharmacokinetic parameters for simulation were derived from the results of a previous study (Anesth Analg 2012; 115: 284-96). Based on the results from a previous study of remimazolam, we assumed log-normally distributed interindividual variances of 10%, 25%, 50%, 80% and 50% for the parameters E_0, E_{min}, EC_{50}, γ and k_{e0}, respectively, and an additive residual intraindividual error with a variance of 25. The simulated data were analyzed by population analysis and the obtained parameter estimates were compared with the "true" parameter values used for simulation. This procedure was repeated 100 times and the power of the population analysis for each parameter was defined as the proportion of runs which showed a relative percentage deviation of the parameter estimate from the true value within the range from -25% to 25%. These simulations revealed that 20 subjects were needed to reach a power of at least 0.8 for each pharmacodynamic parameter.

S5: Prediction probability of MOAA/S for beta-ratio and Narcotrend index

The beta-ratio and Narcotrend index values are shown in figure S5F1 as a function of Modified Observer's Assessment of Alertness and Sedation (MOAA/S) scores in each volunteer. On average, beta-ratio showed a monotonic decreasing function, whereas Narcotrend index did not for MOAA/S scores from 2 to 0. The average prediction probability for beta-ratio was 0.79 and for Narcotrend index 0.74.

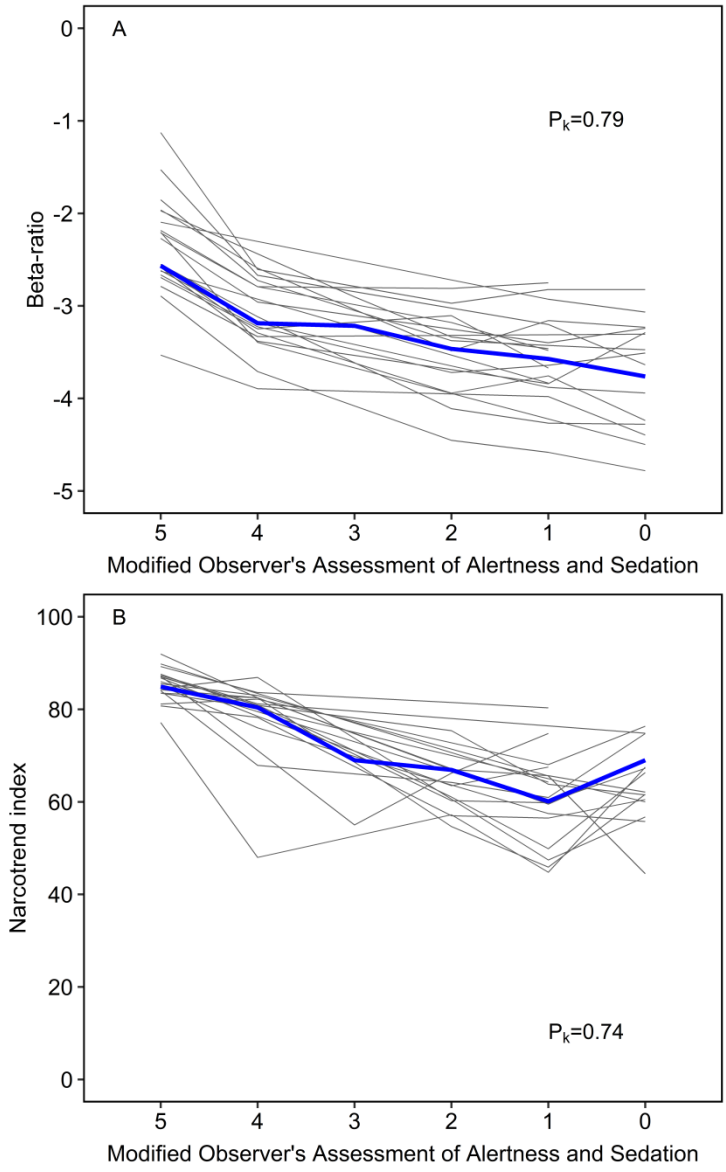

Fig. S5F1: Plot of beta-ratio (A) and Narcotrend index (B) vs. MOAA/S scores. The MOAA/S score observations and the corresponding values of beta-ratio or Narcotrend index immediately before the MOAA/S assessment in each volunteer are plotted as grey lines. Median over individual beta-ratio or Narcotrend index values is shown in blue. P_k: prediction probability

S6: Results of the pharmacodynamic modeling of beta-ratio

A standard sigmoid model was fitted to the data:

$$E = E_0 - (E_0 - E_{min})\frac{C_E^{\gamma}}{C_E^{\gamma} + EC_{50}^{\gamma}} \qquad \frac{dC_E}{dt} = k_{e0} \cdot (C_P - C_E)$$

The individual parameters of the best pharmacokinetic model of remimazolam were used to calculate the plasma and effect site concentrations.

This model showed already a quite high goodness of fit without any bias and relatively small prediction errors (figure S6F1).

The shrinkage of the empirical Bayesian estimates was below 10% for all parameters, indicating that the individual data were sufficiently informative for covariate analysis by linear regression.

Regression plots of the individual parameter estimates revealed no statistical significant effects of the covariates. However, there were weak effects of age on k_{e0} and E_{min} (figure S6F2), of body weight on γ (figure S6F3), and of BMI on EC_{50} and γ (figure S6F4).

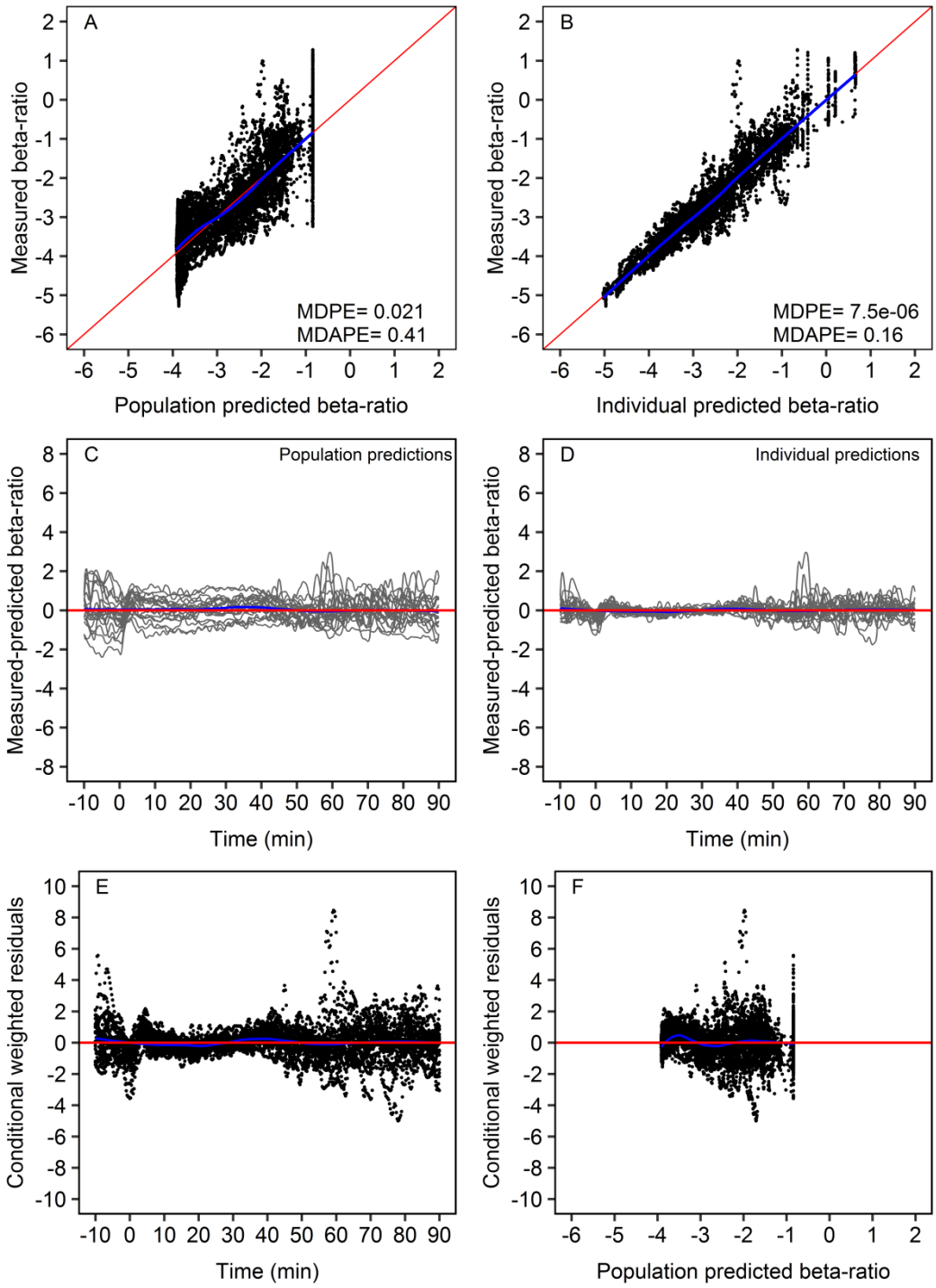

Fig. S6F1: *Diagnostic plots for the basic pharmacodynamic model of beta-ratio. The red lines represent lines of identity (measured=predicted), the blue lines are smoothers through the data. MDPE, median prediction error; MDAPE, median absolute prediction error.*

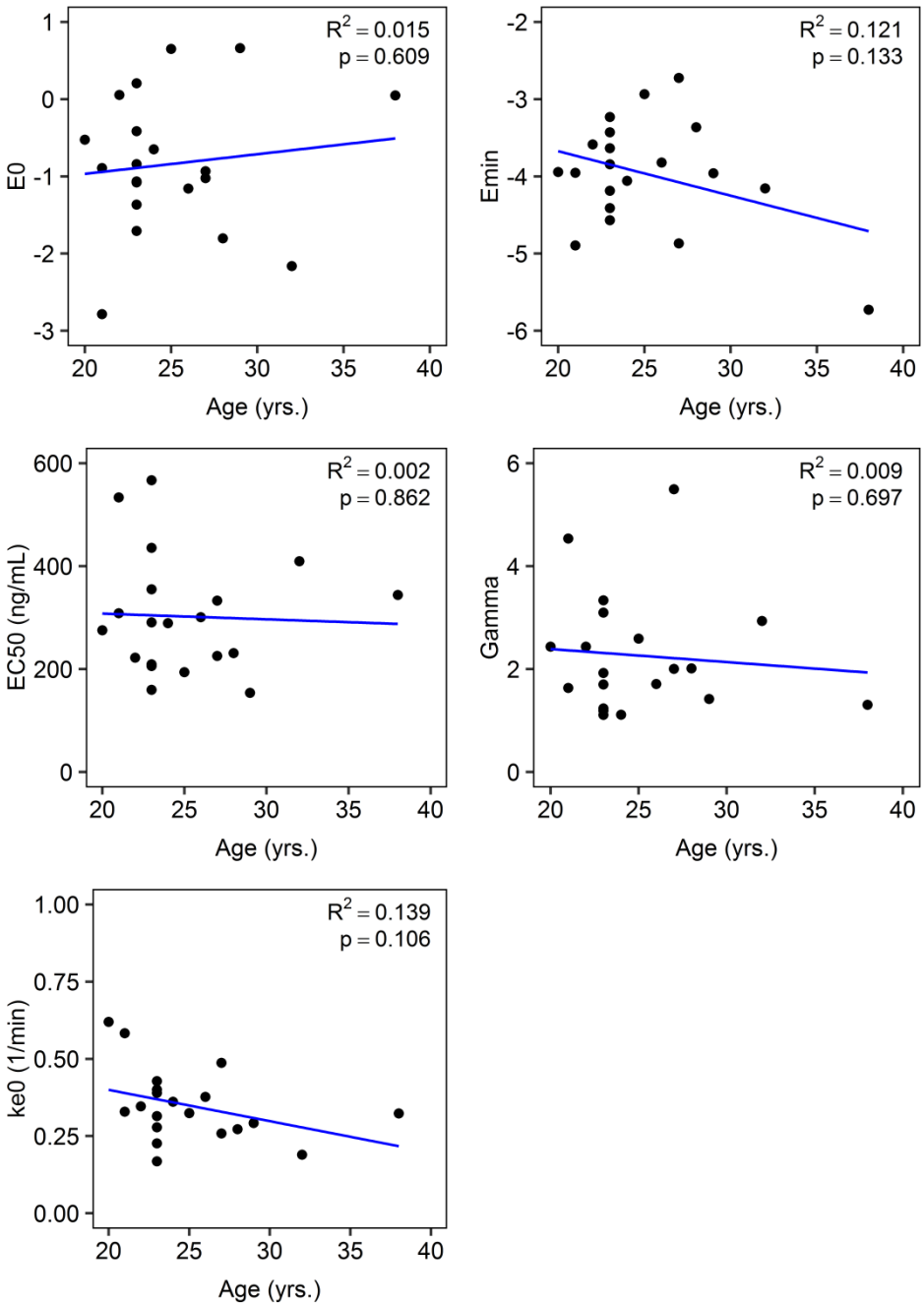

Fig. S6F2: *Plots of the individual parameter estimates vs. age for the basic pharmacodynamic model of beta-ratio. The blue lines represent linear regressions through the data. R^2, regression coefficient; p, significance level of the linear regression; E_0, baseline value of the beta-ratio; E_{min}, minimum value of the beta-ratio; EC_{50}, half-maximum effect site concentration; k_{e0}, effect-site equilibration rate constant.*

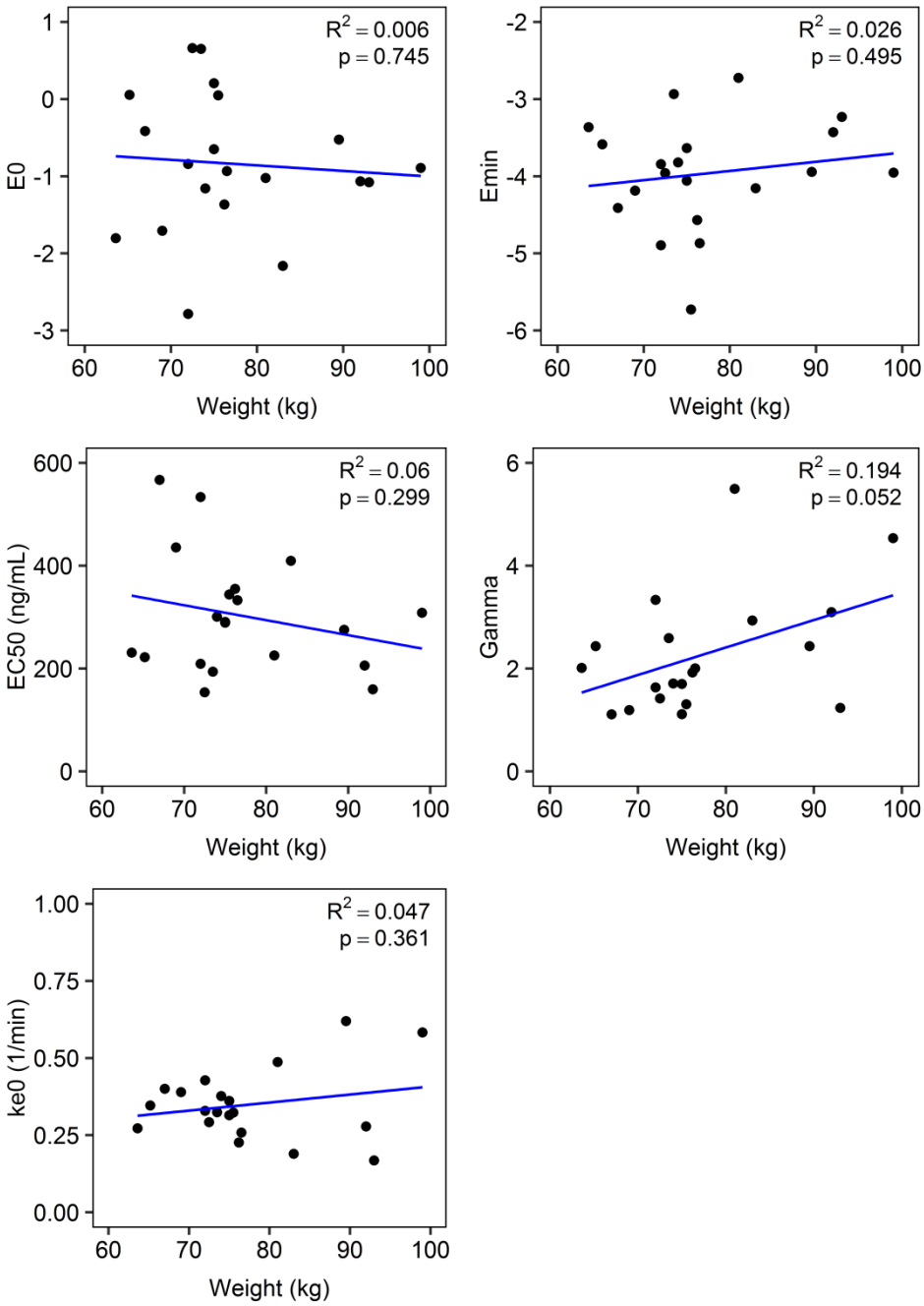

Fig. S6F3: *Plots of the individual parameter estimates vs. body weight for the basic pharmacodynamic model of beta-ratio. The blue lines represent linear regressions through the data. R^2, regression coefficient; p, significance level of the linear regression; E_0, baseline value of the beta-ratio; E_{min}, minimum value of the beta-ratio; EC_{50}, half-maximum effect site concentration; k_{e0}, effect-site equilibration rate constant.*

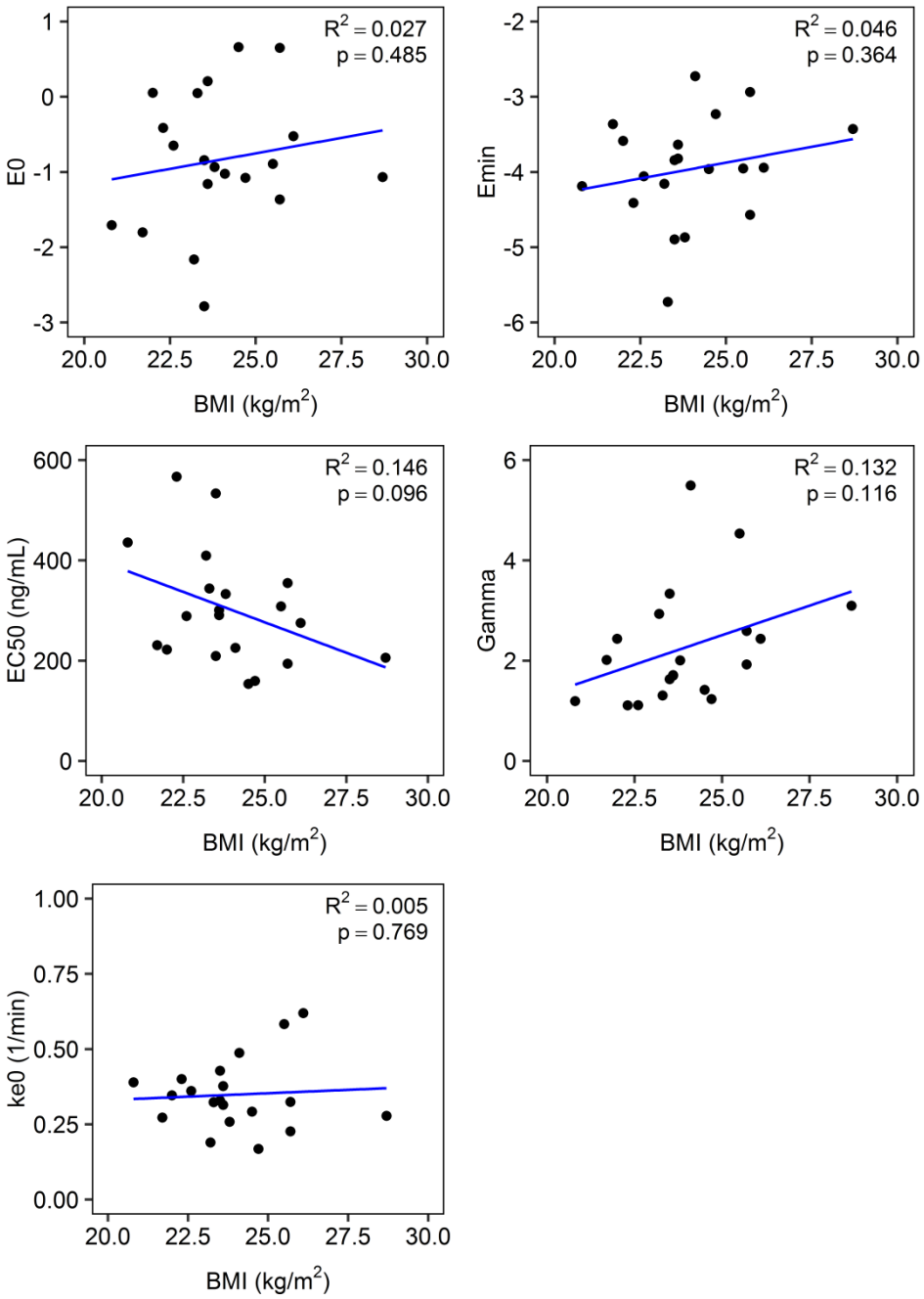

Fig. S6F4: *Plots of the individual parameter estimates vs. BMI for the basic pharmacodynamic model of beta-ratio. The blue lines represent linear regressions through the data. R^2, regression coefficient; p, significance level of the linear regression; E_0, baseline value of the beta-ratio; E_{min}, minimum value of the beta-ratio; EC_{50}, half-maximum effect site concentration; k_{e0}, effect-site equilibration rate constant.*

These covariate effects were therefore tested with the Stepwise Covariate Model (SCM) building tool of the software package PsN. This analysis revealed as best covariate model a linear increase of γ with BMI:

$$\gamma_i = \gamma_{TV} \cdot (1 + \gamma_{BMI}) \cdot (BMI - 23.6)$$

The effect of age on Emin and ke0 was best modeled by combinations of two linear functions:

$$Emin_i = Emin_{TV} \cdot (1 + E_{min}Age1) \cdot (age - 23)\ if\ age \leq 23$$

$$Emin_i = Emin_{TV} \cdot (1 + E_{min}Age2) \cdot (age - 23)\ if\ age > 23$$

$$ke0_i = ke0_{TV} \cdot (1 + k_{e0}Age1) \cdot (age - 23)\ if\ age \leq 23$$

$$ke0_i = ke0_{TV} \cdot (1 + k_{e0}Age2) \cdot (age - 23)\ if\ age > 23$$

When comparing the basic model and this best covariate model the OFV decreased from -8300.3 (BIC= -8201.4) to -8318.2 (BIC= - 8201.3). However, the values for the parameters k_{e0}Age2, E_{min}Age1, und E_{min}Age2 had to be fixed. Additionally, the LLP indicated some problems with the covariate effect parameters (no clear minimum). Therefore, the basic model without covariates was accepted as best model. Figure S6F5 shows the individual measured values of beta-ratio together with the individual and population predictions. The LLP demonstrated that the parameters were estimated reliably (figure S6F6), and the median parameter values of the bootstrap analysis and the confidence intervals obtained by bootstrap analysis and LLP were in good agreement with the estimates of the fit.

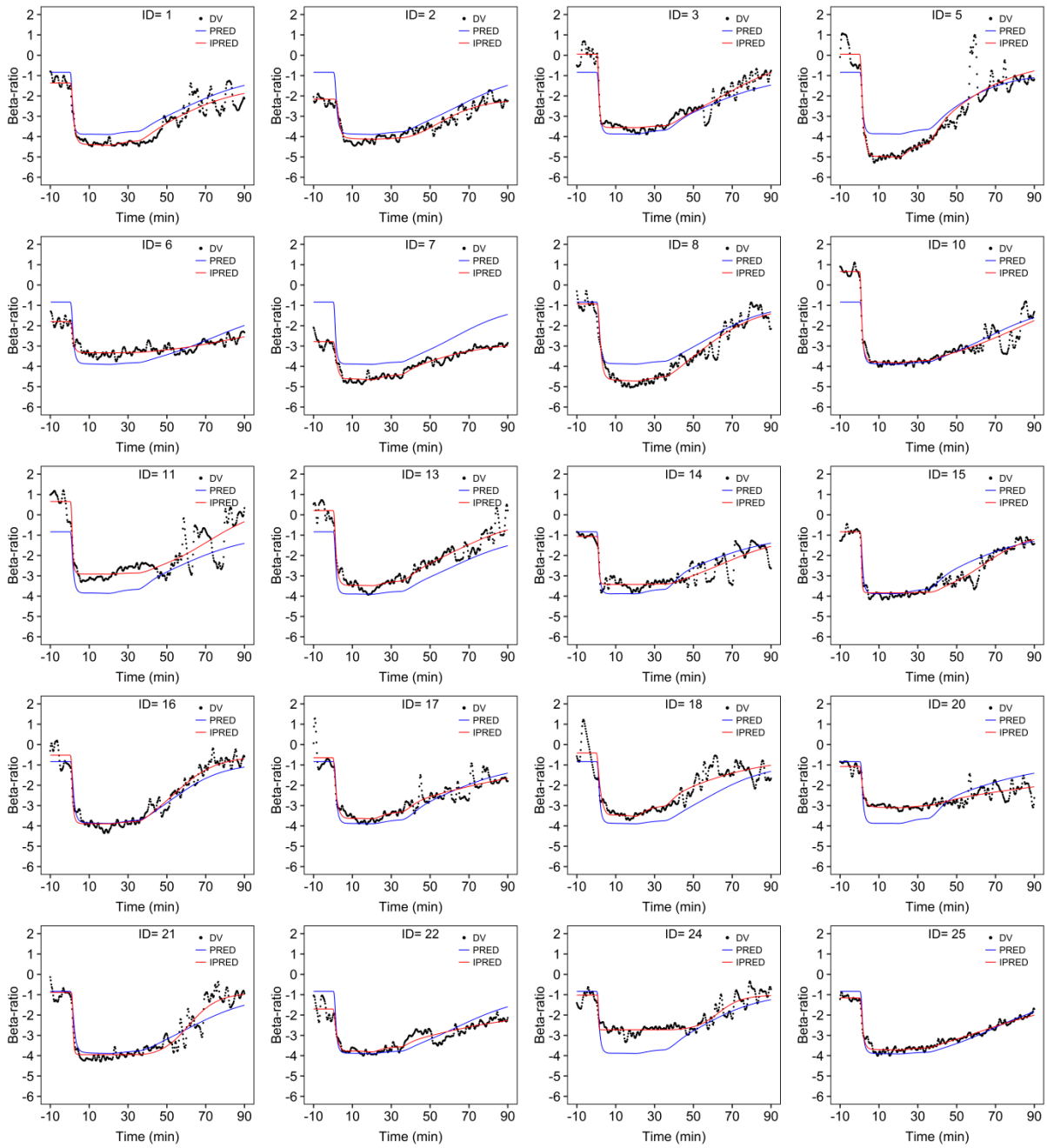

Fig. S6F5: *Individual time courses of measured values (DV), individual predictions (IPRED) and population predictions (PRED) of beta-ratio for the final pharmacodynamic model.*

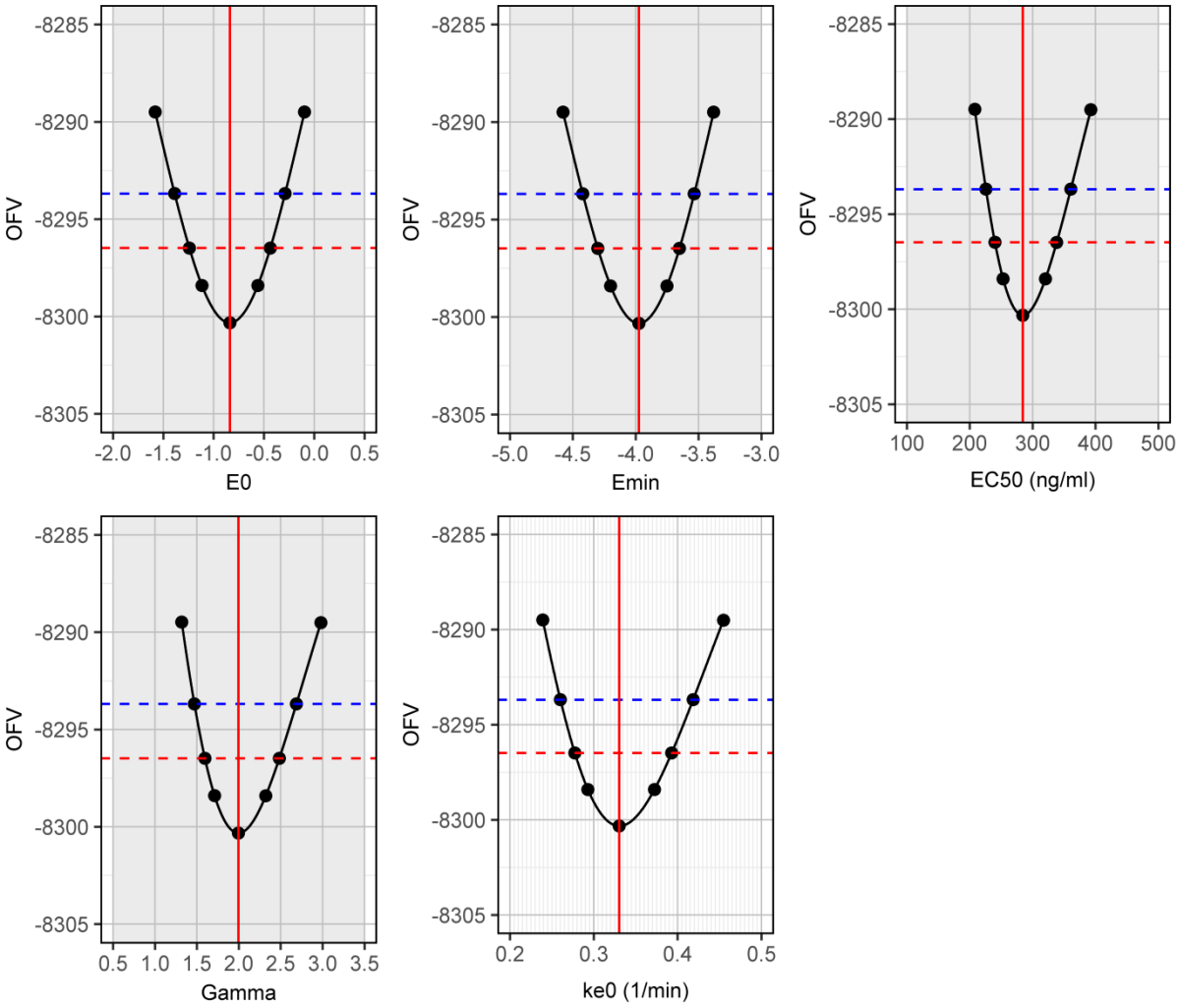

Fig. S6F6: *Log-likelihood profiles for the final pharmacodynamic model of beta-ratio. Critical values of the objective function value are shown as red and blue dotted line for $p<0.05$ and $p<0.01$, respectively. The vertical red line marks the population estimate of the parameter. OFV, objective function value; E_0, baseline value of the beta-ratio; E_{min}, minimum value of the beta-ratio; EC_{50}, half-maximum effect site concentration; Gamma, steepness of the concentration-effect curve; k_{e0}, effect site equilibration rate constant.*

S7: Results of the pharmacodynamic modeling of Narcotrend index

As the standard sigmoid E_{max} model failed to describe the time course of the Narcotrend index, we extended the standard sigmoid model by adding a second sigmoid term with a second effect site concentration:

$$E = E_0 - E_{max,1}\frac{C_{E,1}^{\gamma 1}}{C_{E1}^{\gamma 1} + EC_{50,1}^{\gamma 1}} - (E_0 - E_{max,1} - E_{min})\frac{C_{E,2}^{\gamma 2}}{C_{E2}^{\gamma 2} + EC_{50,2}^{\gamma 2}}$$

$$\frac{dC_{E,1}}{dt} = k_{e0,1} \cdot (C_P - C_{E,1})$$

$$\frac{dC_{E,2}}{dt} = k_{e0,2} \cdot (C_P - C_{E,2})$$

When performing a population analysis NONMEM had problems to estimate the model parameters reliably. As the Narcotrend index data were sampled in a rich design with about 1000 values per subject, it was, however, possible to perform single-subject fits to obtain individual parameter estimates. The parameter estimates from the individual fits are summarized in table S7T1. The parameter γ_1 which describes the steepness of the first sigmoid term was generally extremely high and had to be fixed in some cases to avoid numerical difficulties. In some cases, the minimum effect E_{min} was also fixed as it could not be estimated reliably and showed a high correlation with $EC_{50,2}$. In two subjects the standard sigmoid model without a second sigmoid term was able to describe the data appropriately, as the Narcotrend index of these subjects did not show the typical two phases. In one subject, the effect site equilibration rate constant $ke_{0,1}$ reached the upper boundary of 10, indicating that there was apparently no hysteresis for the initial decrease of Narcotrend index.

The best population fit was obtained when all interindividual variances were set to zero (naïve pooled fit). The diagnostic plots and the individual Narcotrend index data together with individual and population predictions are presented in figures S7F1 and S7F2. Both the

individual fits and the naïve pooled population fit showed an acceptable precision. The LLP demonstrated that the population parameters from the naïve pooled fit were estimated reliably (figure S7F3). As a full population fit could not be performed reliably, a visual predictive check could not be performed.

Table S7T1: Individual estimates for the extended pharmacodynamic model for Narcotrend index, obtained from single fits.

ID	E0	$E_{max,1}$	$EC_{50,1}$ (ng/ml)	γ_1	$k_{e0,1}$ (min^{-1})	E_{min}	$EC_{50,2}$ (ng/ml)	γ_2	$k_{e0,2}$ (min^{-1})
1	93	21	541	465	0.25	45	656	18	0.020
2	94	24	577	212	0.11	40 (fixed)	620	6.7	0.020
3	94	16	317	429	0.32	49	390	140	0.010
5	92	18	359	13	0.17	-	-	-	-
6	89	16	575	588	0.30	41	869	8	0.030
7	86	10	450	99	0.42	64	785	99	0.029
8	98	26	531	26	1.47	53	500	36	0.015
10	87	12	435	100 (fixed)	0.10	47	652	99	0.028
11	96	19	450	100 (fixed)	0.29	30	667	13	0.035
13	100	22	714	97	0.90	25 (fixed)	737	6	0.021
14	96	18	231	8	0.15	45	575	499	0.019
15	98	23	353	99	0.37	41	542	10	0.021
16	98	25	378	6	0.40	36	726	57	0.026
17	100	22	607	108	0.71	30 (fixed)	619	4	0.022
18	89	18	387	24	10	43	826	29	0.040
20	99	19	287	96	0.20	30 (fixed)	376	11	0.011
21	99	19	476	100 (fixed)	0.65	20	544	17	0.013
22	95	12	123	261	0.27	-	-	-	-
24	99	19	454	226	0.32	30 (fixed)	534	19	0.015

25	93	33	811	7	0.54	44	655	123	0.017
Mean	**95**	**20**	**453**	**153**	**0.89**	**40**	**626**	**66**	**0.022**
SD	**4**	**5**	**162**	**166**	**2.15**	**11**	**135**	**117**	**0.008**
Minimum	**86**	**10**	**123**	**6**	**0.10**	**20**	**376**	**4**	**0.010**
Median	**96**	**19**	**450**	**100**	**0.32**	**41**	**636**	**18**	**0.021**
Maximum	**100**	**33**	**811**	**588**	**10**	**64**	**869**	**499**	**0.040**

E_0, baseline value of the Narcotrend index; $E_{max,1}$, maximum inhibitory effect of the first sigmoid term; $EC_{50,1}$: half-maximum effect site concentration of the first sigmoid term; γ_1, steepness of the concentration-effect curve of the first sigmoid term; $k_{e0,1}$: first effect site equilibration rate constant; E_{min}, minimum value of the Narcotrend index; $EC_{50,2}$, half-maximum effect site concentration of the second sigmoid term; γ_2, steepness of the concentration-effect curve of the second sigmoid term; $k_{e0,2}$, second effect site equilibration rate constant.

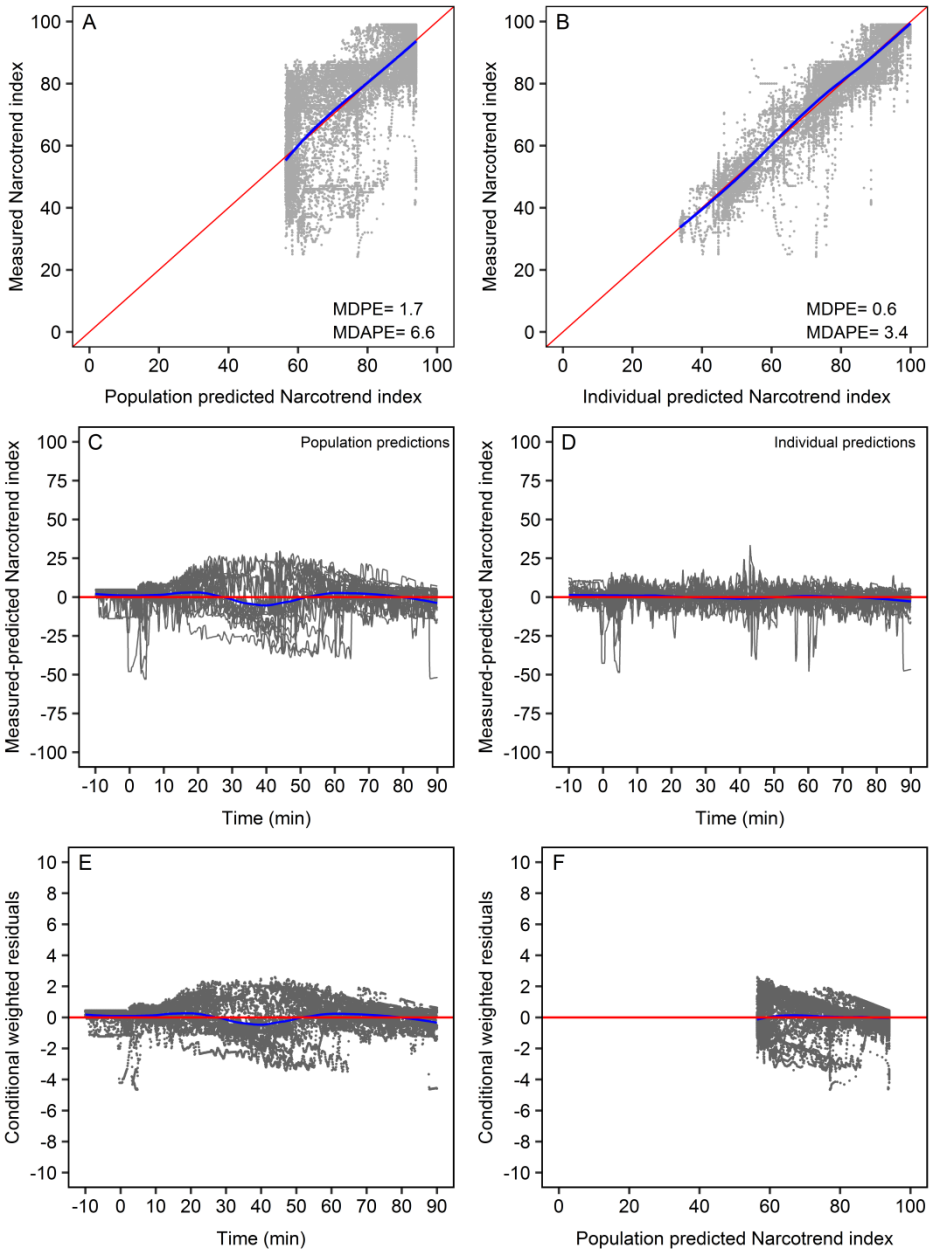

Fig. S7F1: *Diagnostic plots for the extended pharmacodynamic model of Narcotrend index. The red lines represent lines of identity (measured=predicted), the blue lines are smoothers through the data. MDPE, median prediction error; MDAPE, median absolute prediction error.*

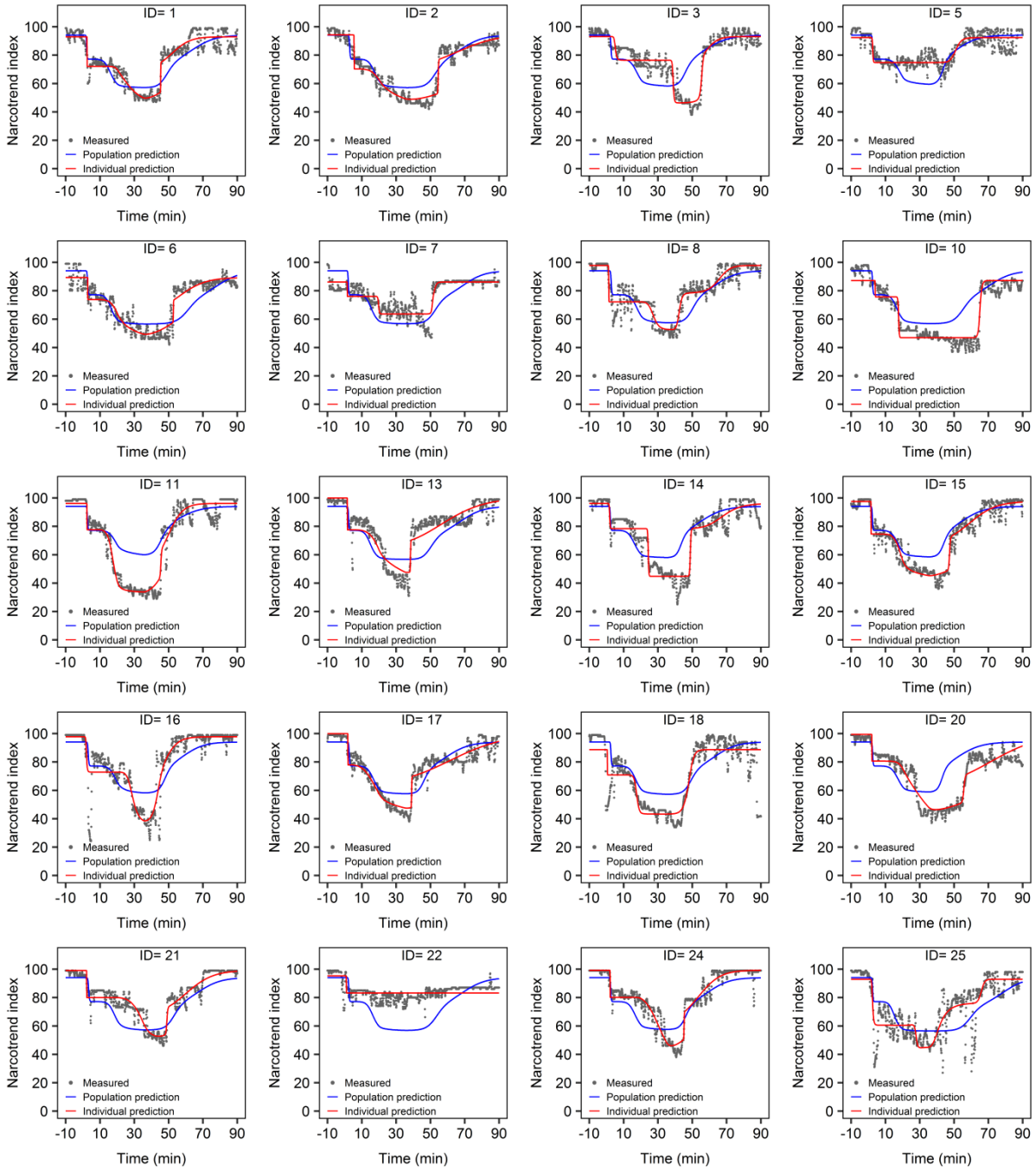

Fig. S7F2: *Individual time courses of measured and predicted Narcotrend index.*

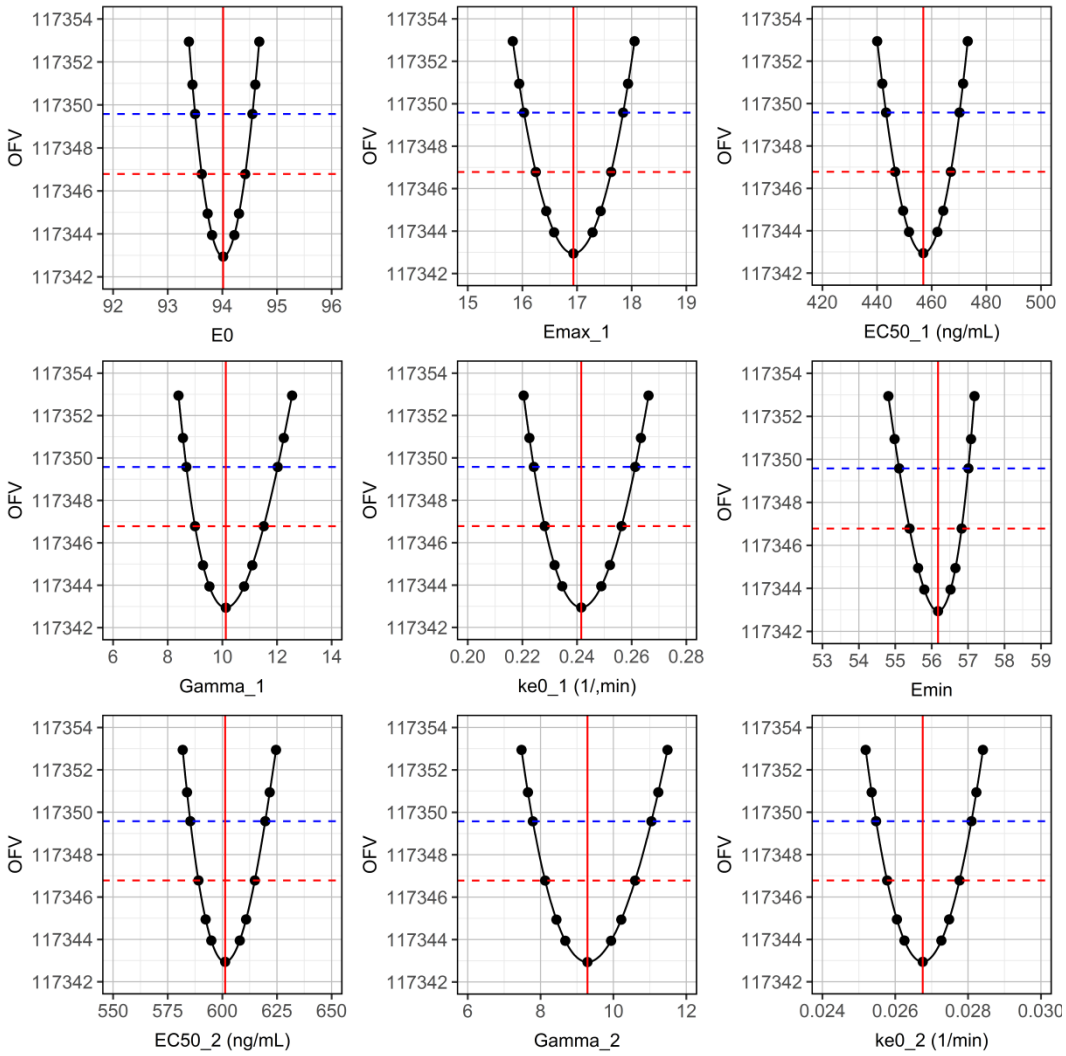

Fig. S7F3: *Log-likelihood profiles for the naïve pooled fit of the extended pharmacodynamic model of the Narcotrend index. Critical values of the objective function value are shown as red and blue dotted line for p<0.05 and p<0.01, respectively. The vertical red line marks the population estimate of the parameter.* E_0*, baseline value of the Narcotrend index;* E_{max_1}*, maximum inhibitory effect of the first sigmoid term;* EC_{50_1}*, half-maximum effect site concentration of the first sigmoid term; Gamma_1, steepness of the concentration-effect curve of the first sigmoid term;* k_{e0_1}*, first effect site equilibration rate constant;* E_{min}*, minimum value of the Narcotrend index;* EC_{50_2}*, half-maximum effect site concentration of the second sigmoid term; Gamma_2, steepness of the concentration-effect curve of the second sigmoid term;* k_{e0_2}*, second effect site equilibration rate constant; OFV, objective function value.*